PAPER

MOF@Cell: 3D printed biobased filters anchored with a green metal–organic framework for effluent treatment†

Natalia Fijoł, [ID] [ab] Andreas Mautner, [ID] [cd] Erik Svensson Grape, [ID] [a] Zoltán Bacsik,[a] A. Ken Inge [ID] [a] and Aji P. Mathew [ID] *[ab]

Multifunctional, biobased materials processed by means of additive manufacturing technology can be highly applicable within the water treatment industry. This work summarizes a scalable and sustainable method of anchoring a green metal–organic framework (MOF) SU-101 onto the surface of 3D printed, biobased matrices built of polylactic acid (PLA)-based composites reinforced with TEMPO-oxidized cellulose nanofibers (TCNFs). The two tested anchoring methods were hydrolysis *via* either concentrated hydrochloric acid treatment or *via* a photooxidation reaction using UV–ozone treatment. Stable deposition of SU-101 distributed homogenously over the filter surface was achieved and confirmed by FT-IR, XPS and SEM measurements. The obtained 3D printed and functionalized MOF@PLA and MOF@TCNF/PLA (aka MOF@Cell) filters exhibit high efficiency in removing heavy metal ions from mine effluent and methylene blue from contaminated water, as demonstrated through batch adsorption experiments. In addition to their potential for removal of contaminants from water, the MOF@Cell filters also exhibit excellent mechanical properties with a Young's modulus value of about 1200 MPa, demonstrating their potential for use in practical water treatment applications. The MOF@Cell filters were able to maintain their structural integrity and filtration performance even after multiple cycles of use and regeneration. This study highlights the potential of multifunctional, biobased materials processed by additive manufacturing technology as a cost-effective alternative to traditional water treatment methods. The MOF@Cell filters presented in this study demonstrate high efficiency, durability, and reusability, making them promising candidates for practical applications in the modern water treatment industry.

1. Introduction

Metal ions constitute a serious hazard to the environment, as they are non-biodegradable,[1] bioaccumulative[2] and toxic[3] to the extent of being carcinogenic.[4] Consequently, their levels in environmental water reservoirs need to be carefully measured and controlled on a strict regular basis. Human activities in *i.a.* metallurgical and mining industries vastly contribute to the pollution of the world's waters and soils with metal ions. In Europe, the wastewater effluents from mines are one of the main causes of water pollution. The most commonly reported metal ion pollutants include cadmium (Cd),[5,6] lead (Pb),[5–7] zinc (Zn),[5–7] manganese (Mn),[6] copper (Cu)[6,7] and arsenic (As).[8]

Treatment technologies for metal ion removal from wastewater include filtration,[9] sedimentation,[10] precipitation,[11] ion exchange[12] and adsorption.[13] Adsorption, due to its high efficiency and ease of operation, is extensively used worldwide[14–18] with the most commonly used adsorbents being alumina[19] and alumina-based materials,[20–22] silica[23] and silica-based materials[24,25] as well as adsorbents based on activated carbon.[26–28] However, in line with the progressing climate crisis and the prospect of secondary pollution issues, it is crucial to introduce renewable biomaterials that could successfully replace conventional, non-renewable adsorbents.

Metal–organic frameworks (MOFs) are a class of widely applied crystalline porous materials shaped by joining metal centres or clusters with organic molecules, forming framework-type structures exhibiting high porosities. They have attracted vast research interest over the past two decades due to their incredibly high specific surface areas and modular nature,[29]

[a]Department of Materials and Environmental Chemistry, Stockholm University, Frescativägen 8, 106 91, Stockholm, Sweden. E-mail: aji.mathew@mmk.su.se; Tel: +46 8161256

[b]Wallenberg Wood Science Center, Teknikringen 56-58, 100 44, Stockholm, Sweden

[c]Polymer and Composite Engineering (PaCE) Group, Institute of Materials Chemistry and Research, Faculty of Chemistry, University of Vienna, Währinger Str. 42, 1090, Wien, Austria

[d]Institute for Environmental Biotechnology, Department IFA, University of Natural Resources and Life Sciences Vienna, Konrad-Lorenz-Straße 20, 3430 Tulln an der Donau, Austria

† Electronic supplementary information (ESI) available. See DOI: https://doi.org/10.1039/d3ta01757e

12384 | *J. Mater. Chem. A*, 2023, **11**, 12384–12394

This journal is © The Royal Society of Chemistry 2023

allowing for tuning of properties for applications within *e.g.* catalysis and chemical sensing. Additionally, promising performance has been shown within environmental applications, including both adsorption of gases and the sequestration of environmental pollutants including various metal ions[30–32] from water. A novel, bioinspired microporous MOF, SU-101, made from a plant-sourced organic molecule *i.e.* ellagic acid,[33] synthesized in an aqueous suspension at room temperature, could be an environmentally friendly alternative to conventional MOFs used so far for water treatment applications. Moreover, anchoring SU-101 onto biobased matrices by *i.a.* an integrated 3D printing process could add robustness and mechanical stability to filtration systems based on such MOFs, enable more structured and facile removal of adsorbed species (by simple acid desorption of a MOF together with adsorbed contaminants, all while keeping the bioplastic matrix intact and instantly available for re-functionalization) as well as enhance the recycling of the adsorbent (which can be performed separately by chemical or physical treatments).

Fused deposition modelling (FDM) is a 3D printing technology of choice for the development of biobased matrices for anchoring of adsorbent species. FDM offers various benefits when compared to traditional manufacturing methods, as it is relatively inexpensive, operates at high speed, generates low material losses and most importantly, enables the development of customized and complex shaped filtration systems at the point and time of need.[34–36] Polylactic acid (PLA) is a biodegradable polymer material often used for FDM. PLA can be easily processed by using commercial, desktop 3D printers and its use results in 3D prints of high resolution and excellent finish quality.[37] Moreover, it presents an alternative to nonrenewable synthetic polymers commonly used within the 3D printing industry, as PLA is biodegradable and it can be obtained from renewable resources such as sugarcane and corn.[38] Compounding PLA with various nanoparticles yields 3D printed parts with improved properties. A wide variety of nanospecies was proposed including nanocarbon,[39] hydroxyapatite[40] and nanocellulose particles,[41–43] *e.g.* 2,2,6,6-tetramethylpiperidine-1-oxyl (TEMPO)-oxidized cellulose nanofibers (TCNFs). As reported in our previous work,[36] using TCNFs as a reinforcement in PLA results in enhancement of the mechanical performance of the 3D printed water purification filters, and improves adsorption performance of PLA-based filters towards removal of metal ions from water.

This study aims to surface-functionalize 3D printed, biocomposite-based water purification filters with a green MOF – SU-101. The functionalized filters include two different 3D printed shapes *i.e.* (i) a PLA filter fabricated with the use of a commercially available 3D printing filament referred to as MOF@PLA and the (ii) PLA-based filter reinforced with TEMPO-oxidized cellulose nanofibers (TCNFs) fabricated with the in-house developed biocomposite filament referred to as MOF@-Cell. The development of the biobased TCNF/PLA 3D-printing filament and further utilization thereof to fabricate variously shaped water purification filters suitable for removal of metal ions and microplastics from water is reported in our previous work.[36] The previous study established satisfactory performance

of the 3D printed PLA and TCNF/PLA filters for adsorption of Cu^{2+} ions. However, in order to achieve a highly efficient water filter, further functionalization thereof with the robust and biocompatible SU-101 material aims to improve the overall metal ion adsorption properties *via* enabling more selective adsorption, which could lead to a wider applicability of 3D printed filters within the water treatment industry.

2. Experimental

2.1 Materials and methods

Raw materials used included transparent, extrusion grade PLA pellets (Ingeo™ Biopolymer 4043D, Nature Works, provided by Add North 3D AB, Sweden), 1,4-dioxane (anhydrous, 99.8%, Carlo Erba Reagents, Spain), hydrochloric acid (37%, VWR International, Germany), nitric acid (65%, VWR International, France), TEMPO (2,2,6,6-tetramethylpiperidine-1-oxyl radical)-mediated oxidized cellulose nanofibers (TCNFs, 1.1 mmol g^{-1} of carboxyl groups, provided by Swiss Federal Laboratories for Materials Science and Technology (EMPA), Switzerland). The dimensions of nanofibers, as studied by atomic force microscopy, were in the range of 3–5 nm and lengths in the μm scale.[44] The commercial 3D printing filament used for printing out reference models was a transparent PLA filament with a diameter of 2.85 mm (Add North, 3D AB, Ölsremma, Sweden). The MOF powder was prepared from ellagic acid (sold as a dietary supplement pomegranate extract, PureBulk Ltd, 90% ellagic acid) and bismuth acetate (Alfa Aesar, 99%).

Preparation of TCNF/PLA composites. The master batch of the composite suspension was prepared using the protocol reported in our previous studies.[36,45] In brief, transparent, commercial PLA pellets were dissolved in 10 vol% of 1,4-dioxane solution and magnetically stirred overnight for 12 h at room temperature *i.e.* at 18–20 °C. The TCNF gel was added to the suspension and magnetically stirred for 2 h. The PLA/1,4-dioxane/TCNF viscous suspension was then added drop-wise into liquid nitrogen forming the TCNF/PLA pellets (5 wt% TCNF content). The pellets were freeze dried for 48 h in order to remove excess solvent and then single-screw extruded into 3D printing filaments with a diameter of 2.85 mm at a feed temperature of 180 °C and screw speed of 100 rpm.

Preparation of the metal–organic framework (MOF). The SU-101 powder was prepared by adding ellagic acid and bismuth acetate to a mixture of water and acetic acid (6 vol% acetic acid) at room temperature, as per a previously published procedure.[33] The acquired solid was then filtered, dried overnight at 60 °C in air, and used without further purification.

3D printing. All of the prototypes were based on cubic computer-aided design (CAD) models. The dimensions and pore architecture were adjusted with the use of CURA slicing software prior generating the G-code file necessary for being processed by the printer (Ultimaker S5, Ultimaker BV, The Netherlands). The printing parameters used for the biocomposite and the reference commercial PLA filaments were: nozzle diameter 400 μm, print bed temperature 60 °C, printing speed 45 mm s^{-1}, layer thickness 150 μm, shell thickness 500 μm, infill density: 10%, infill line distance: 1.5 mm, infill

This journal is © The Royal Society of Chemistry 2023

J. Mater. Chem. A, 2023, **11**, 12384–12394 | **12385**

pattern: grid, wall thickness: 0.5 mm, printing speed: 45 mm s^{-1}. The nozzle temperature was set to 200 °C and 215 °C for PLA and TCNF/PLA, respectively. Two different models were printed: (i) cuboid models ($15 \times 15 \times 5$ mm) were used for the optimization of the anchoring procedure as well as for the batch adsorption studies and (ii) cuboid models ($25.4 \times 12.7 \times 12.7$ mm) were used for compression testing.

Anchoring procedure. 3D printed cuboid prototypes ($15 \times 15 \times 5$ mm) were surface functionalized with the SU-101 MOF. The anchoring procedure included the activation of PLA with either a 5 h acid bath (10 M HCl) or a UV-ozone treatment for 10 min (UV/Ozone ProCleaner™, Bioforce Nanosciences, USA). The activated samples were then immersed in a 1% SU-101 suspension and stirred overnight for 12 h at 45 °C. Then, the samples were rinsed with deionized water to remove the excess of unattached MOF, followed by oven drying at 70 °C for 1 h and air-drying for 24 h.

Size exclusion chromatography. Analysis of the molecular weight (M_w) and the molecular weight distribution (MWD) of the reference as well as acid- and ozone-activated samples was performed with SEC (Malvern Instruments, Malvern, UK). The separation was carried out on a double, 5 μm PLgel, MIXED-D column. Chloroform with a flow rate of 0.5 mL min^{-1} was used as the eluent. The entire experiment was carried out at 35 °C.

Fourier-transform infrared spectroscopy (FTIR). The filters before and after the anchoring procedure as well as before and after the adsorption study were analysed by infrared spectroscopy (610 IR FT-IR spectrometer, Varian Inc., CA, USA) equipped with a Specac Golden Gate single reflection attenuated total reflection (ATR) accessory with a diamond ATR element (Specac, UK). Sixteen scans between 4000 cm^{-1} and 400 cm^{-1} were averaged for each spectrum at intervals of 1 cm^{-1}.

Scanning electron microscopy (SEM). The morphology and the distribution of the MOF on the 3D printed filters was imaged with the use of a Hitachi TM3000 tabletop microscope (Hitachi Ltd, Japan). The samples were investigated using an accelerating voltage of 5 kV and 15 kV in back-scattered electron mode.

X-ray diffraction (XRD). Powder X-ray diffraction (PXRD) data of the as-synthesized MOF and the filter prototypes were acquired using a Panalytical X'pert Pro diffractometer (Cu K$\alpha_{1,2}$, $\lambda_1 = 1.5406$ Å, $\lambda_2 = 1.5444$ Å) using Bragg–Brentano geometry.

Compression testing. Compressive tests were performed according to the Standard Test Method D695-15 on cuboid specimens ($12.7 \times 12.7 \times 25.4$ mm). 5 samples were tested for each type of filter. The samples were conditioned prior to the analysis for 48 h in a conditioning chamber at 23 °C and 51% relative humidity. A 10 kN load cell and a compression rate of 1 mm min^{-1} were applied until 60% deformation was reached. The tests were performed by applying a force perpendicular to the printing direction on an Instron 5960 dual column universal test frame (Instron Corporation, USA) in a controlled environment (23 °C and 51% relative humidity). The apparent compressive elastic modulus was calculated from the slope of the linear elastic section of the stress–strain curves, without considering the plateau and the densification regime. The

energy dissipation, *i.e.* the toughness of the samples, was calculated considering the area under the stress–strain curve.

X-ray photoelectron spectroscopy (XPS). XPS analysis for the 3D-printed PLA and TCNF/PLA filters before and after functionalization by acid and ozone treatment was conducted using an Axis Ultra DLD electron spectrometer (Kratos Analytical Ltd, UK) (K-alpha, monochromated, Al Kα radiation) with a pass energy of 160 eV, an analysis area of 300 μm $\times$ 700 μm, and an energy step size of 1 eV for the survey spectrum (5 scans). The high-resolution spectra (step size 0.1 eV) of the single elements were acquired with 3–10 scans at pass energies of 20 eV.

Thermogravimetric analysis (TGA). The thermal decomposition of the functionalized filters and their corresponding reference starting materials were analysed with the use of a Discovery TGA (TA Instruments Inc., United States). The samples were weighed to fractions of between 15 and 30 mg, placed in high-temperature platinum holders, and then heated from 30 °C up to 550 °C at a heating rate of 10 °C min^{-1} under a nitrogen flow of 20 mL min^{-1}. The weight remaining in the system at 500 °C allowed the amount of MOF anchored on the surface of the filters to be calculated.

Batch adsorption tests. Adsorption tests were conducted using mine wastewater effluent collected at Håkansboda mine, Sweden. The water sample was kindly donated by the IVL Swedish Environmental Research Institute, Stockholm, Sweden. The metal ion adsorption capability of MOF-functionalized filters as well as control PLA filters was assessed by immersing the filters (weighing between 0.9 and 1.1 g) in 150 mL of wastewater effluent. The adsorption tests were conducted under continuous magnetic stirring (450 rpm) at room temperature (18–20 °C). The pH of the effluent water was measured to be in the range between 7.4 and 7.8 and was not controlled or modified within the duration of the adsorption experiment in order to assess the performance of filters under realistic conditions. The filtrate samples with a volume of approximately 25 mL were collected after 1 h and 24 h into 2 vol% of nitric acid (HNO$_3$, 65%, VWR International, France) washed and overnight-soaked vials. The metal concentration in the collected aliquots was assessed with inductively coupled plasma mass spectroscopy (ICP-MS).

Desorption and recyclability tests. The metal ions adsorbed onto the filter's surface were desorbed by immersing the filters in 20% ammonium chloride (NH$_4$Cl) solution at room temperature (18–20 °C) and stirring at 450 rpm for 3 h. After that, the filters were further treated with 10 M HCl for 15 min in order to both remove any remaining metal ions and re-activate the filter's surface prior to the following MOF re-anchoring procedure. The MOF re-anchoring was carried out as described in the Anchoring procedure section with the omission of the surface activation steps.

To further assess the recyclability potential of the filters, they were tested for removal of methylene blue (MB) from water. The same filters which were used for the metal ion adsorption study were tested for dye removal (after triple ion desorption and MOF re-anchoring procedure). The filters were immersed in 80 mL of MB solution (conc. 10 mg L^{-1}) at room temperature (18–20 °C) and stirred at 400 rpm. Aliquots of 20 mL were removed for

12386 | *J. Mater. Chem. A*, 2023, **11**, 12384–12394

This journal is © The Royal Society of Chemistry 2023

analysis after 0.25, 0.5, 1 and 24 hours. The removal efficiency was assessed with an ultraviolet-visible (UV-vis) spectrophotometer (Genesys™, 40/50, ThermoFisher) using the colorimetric method (λ^{max} = 664 nm). The UV-vis calibration curve is presented in Fig. S1.†

Inductively coupled plasma mass spectrometry (ICP-MS). The samples were conserved with HNO_3 to a concentration of 1% and analyzed by ICP-MS according to IVL's method A30 based on SS-EN ISO 17294-2 2016 and SS-EN 14902:2005. The analysis was performed in KED mode with a collisional gas on an ICP-MS (ICAP-Q, Thermo Scientific) with an internal standard of germanium, iridium, rhodium and indium in order to correct matrix effects in the analysis.

Surface zeta potential. The surface charge of the filters was investigated by recording the ζ-potential as a function of pH value with a SurPASS electrokinetic analyzer (Anton Paar, Graz, Austria). The specimens were mounted into an adjustable gap cell with double-sided tape at a gap width of 130 μm. A KCl solution (1 mmol L^{-1}) was used as the electrolyte and the pH value was controlled by titrating HCl and KOH (0.05 mol L^{-1}). The ζ-potential was calculated from the recorded streaming current.

3. Results and discussion

3.1 Surface functionalization of the 3D printed filters

After optimizing and testing various activation processes (Fig. S2†), two different activation mechanisms, which showed the most promise, were applied to the 3D printed PLA and TCNF/PLA filters (Fig. 1). The first method was hydrolysis by immersion of the filters in 10 M hydrochloric acid (HCl). PLA is a hydrophobic polymer and it was previously reported that an acidic environment makes it more hydrophilic by affecting its ester linkages, leading to exposure of the polymer's hydroxyl and carboxyl groups.[46] The second method relied on subjecting the printed filters to a UV-ozone (O_3) treatment. As previously reported by Choi et al.,[47] this type of treatment leads to photooxidation of PLA materials introducing carbonyl groups to the PLA's surface and consequently increasing the surface charge density facilitating various interactions, especially with positively charged species. The increased density of negative

charges on the filter's surface was confirmed by determining the zeta potential of the filters (Fig. 2d). It can be observed that at the experimental pH of mine effluent (i.e. between pH 7.4–7.8) the zeta potential of acid and O_3-activated filters differs from that of the PLA reference filter and reaches more negative values, which is particularly pronounced for the acid-activated filters. The activated PLA and TCNF/PLA filters were further immersed in a 1% SU-101 MOF suspension. It was shown that both the photooxidation reaction as well as the acid hydrolysis of PLA enhances the deposition of SU-101 on the filter's surface. We hypothesize that the interactions between SU-101 and the surface of the filters occur via a variety of different interactions. As the MOF is not charged, the primarily expected mechanism would include physical interactions such as van der Waals interactions; however, due to the exposed hydroxyl and carbonyl groups on the surface of hydrolysed and photooxidized matrices, adsorptive connection cannot be fully excluded. What is more, both acid and ozone treatments lead to roughening of matrix surfaces creating nano- and micro-pores, which could entrap SU-101 molecules on the filters' surfaces. The deposition of SU-101 on the PLA and TCNF/PLA filter surfaces was studied by SEM and SEM-EDX mapping targeting one of the main components of the MOF's structure i.e. Bi. As presented in Fig. 2a, successful deposition was confirmed by the change in colour of the functionalized filters for both the reference PLA and TCNF/PLA filters. The SEM images (Fig. 2b) clearly show a more profound charge-up phenomenon on the filter's surfaces, which can correspond to the thicker deposits of MOF powder, and is particularly pronounced for the O_3 treated PLA and TCNF/PLA filters (denoted as PLA O_3 and TCNF/PLA O_3). Some unevenly distributed small white deposits are even present on the control PLA sample (non-activated filter); however, the SEM-EDX analysis (Fig. 2c) clearly reveals that inducing both types of activation processes on the 3D printed filters increased the deposited load of SU-101 and resulted in a homogeneous distribution of the MOF over the 3D-printed filter surfaces. The exact amount of MOF anchored onto the surface of the 3D printed filters was gravimetrically assessed by comparing the weight of oven-dried MOF@filters to the weight of activated matrices. The amount of anchored SU-101 was averaged to be approximately 10 mg per filter. This was
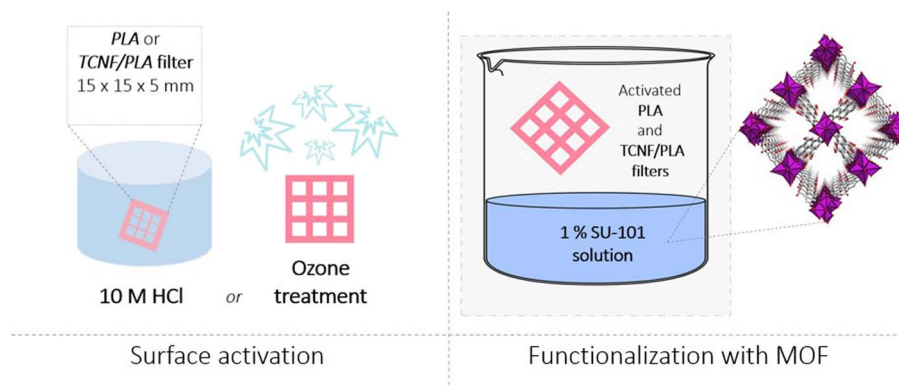

Fig. 1 Overview of the surface functionalization procedure.

This journal is © The Royal Society of Chemistry 2023

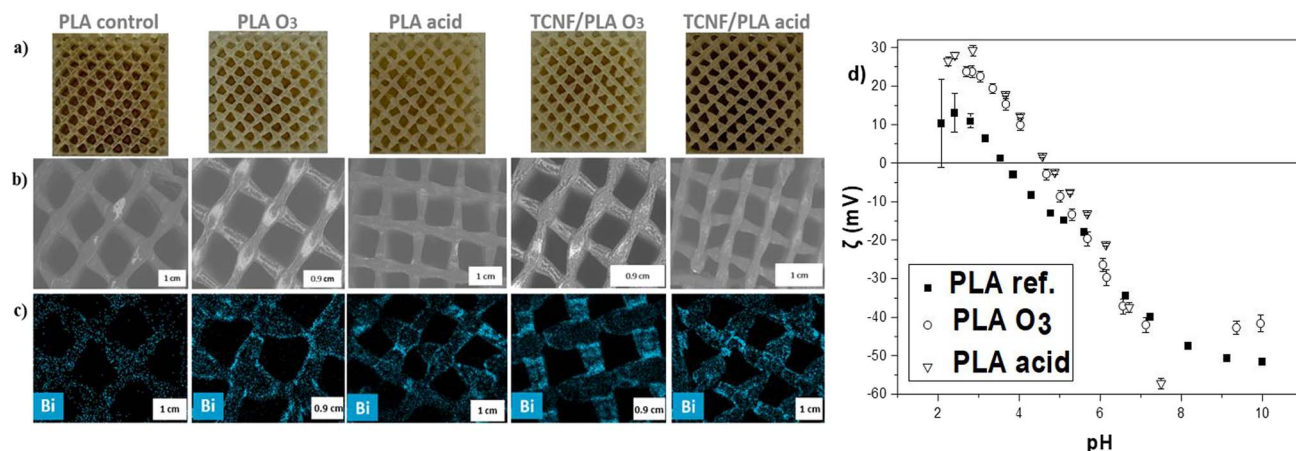J. Mater. Chem. A, 2023, **11**, 12384–12394 | **12387**

Fig. 2 (a) Overview of the functionalized filter's surface, (b) corresponding SEM images, (c) elemental mapping confirming homogenous deposition of the SU-101 MOF over the filter surface, and (d) zeta potential of acid and O_3-activated samples compared to that of the reference PLA filter.

confirmed by the TGA measurements conducted (Fig. S3†). While the ozone-activated filters presented a similar loading of MOF onto their structures, it is noteworthy that acid-activated TCNF/PLA samples showed a nearly twice as high amount of SU-101 present on their surface, indicating a possible role that cellulose nanofibers play in the anchoring procedure.

The deposition of MOF over the 3D printed filters as well as the overall mechanism of the functionalization procedure was further analysed with FT-IR and XPS spectroscopies. The results clearly show interactions between SU-101 and the filter matrix, *i.e.* PLA and TCNF/PLA.

As observed in the IR spectra collected for MOF@ PLA and MOF@TCNF/PLA (aka MOF@Cell) (Fig. 3a), new bands were formed upon functionalization. Both the pristine PLA and reference TCNF/PLA spectrum show bands characteristic of PLA *i.e.* stretching vibrations at 1078 cm^{-1} and 1178 cm^{-1} assigned to C–O groups, and at 1747 cm^{-1} corresponding to C=O functional groups. Bands for C–H bending vibrations in –CH$_3$ and –CH$_2$– groups were observed at 1380 cm^{-1} and 1450 cm^{-1}

and the corresponding C–H stretching vibrations appeared in the region of 2800–3000 cm^{-1}. All of these bands were still present on the IR spectra of the surface functionalized PLA and TCNF/PLA filters; however, new bands originating from the SU-101 chemical structure were observed as well. Sharp and strong bands at 1592 cm^{-1} and 1470 cm^{-1} can be assigned to C=C vibrations in the aromatic ring. Bands in the region of 920–700 cm^{-1} that correspond to aromatic C–H bending vibrations were identified. Clear conclusions about the nature of the interaction between SU-101 and the filters cannot be drawn from the IR spectra.

Furthermore, the successful adhesion of SU-101 crystals to the filters could be validated through powder X-ray diffraction (PXRD) measurements (Fig. 3b), indicating that the O$_3$-activation of the substrates results in a higher loading of MOF crystals. The deposition of SU-101 onto acid-activated filters shows that the MOF is converted into BiOCl.

The effect of both acid and O$_3$ treatment was clearly revealed by XPS. The relative ratios of all C–O–C, C=O and O=C–OH
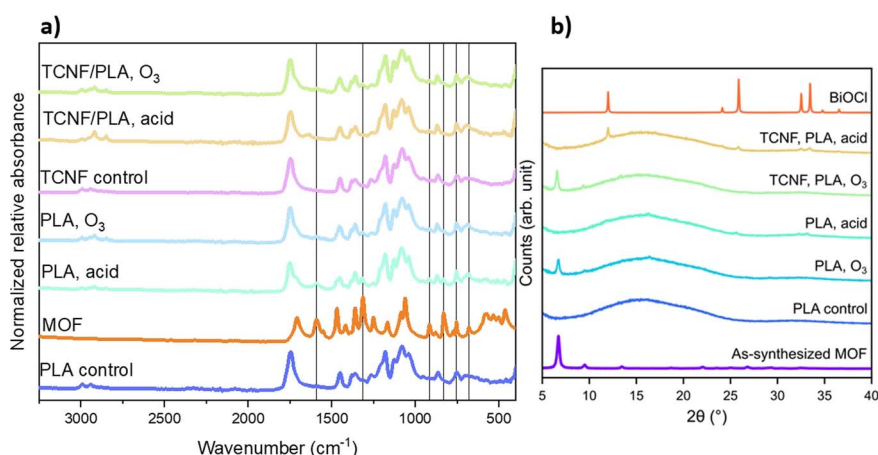

Fig. 3 (a) IR and (b) XRD spectra of the MOF and all of the functionalized filters.

12388 | *J. Mater. Chem. A*, 2023, **11**, 12384–12394

This journal is © The Royal Society of Chemistry 2023

moieties were increased by approximately 50% for O_3 activation and almost doubled in the case of acid treatment confirming the oxidation. Successful oxidation was also confirmed by O contents that increased by approximately one third. Attachment of MOFs onto the surface of the filters was attributed to the introduction of functional groups. XPS also allowed for the estimation of the amount of MOF that was attached. Pure SU-101 exhibits a surface Bi content of 7.7 at%, while Bi contents at the surface were 0.8, 2.8, 1.8 and 1.7 at% for PLA (O_3), PLA (HCl), TCNF (O_3) and TCNF (HCl), respectively. However, the exact mechanism of anchoring needs to be investigated further.

3.2 Mechanical properties of the functionalized filters

The SU-101 functionalized 3D printed PLA and TCNF/PLA specimen and the reference non-functionalized PLA and TCNF/PLA specimen in standardized dimensions (Fig. 4a) and with a uniformly porous structure were subjected to uniaxial compression tests in order to establish whether the acid and O_3 activation has a significant impact on the mechanical performance of the filters. Representative stress–strain curves are presented in Fig. 4b. The linear elastic region of the curves used for calculating the Young's modulus is zoomed in and shown in Fig. 4c. As reported in our previous work,[36] both the elastic modulus and the toughness values of pristine PLA filters were improved by the addition of TCNFs. This study confirms that finding, showing the Young's modulus and average toughness

of the pristine TCNF/PLA samples being 9% and 45% higher when compared to those of the reference and pristine PLA samples, respectively.

However, surface activation of the filters influences their mechanical properties to a lesser extent than expected. The final Young's modulus and toughness values obtained for all of the activated samples are presented in Table S1.† Still, the values remain highly satisfactory and show great potential for using the filters in the designated application i.e. wastewater purification under a direct water flux.

It was shown that the acid treatment resulted in a reduction of the Young's modulus by only 6% for both MOF@PLA and MOF@Cell filters when compared to the non-treated filters. This indicates that both types of filters are affected to the same small degree by the acid treatment, and hence, this stresses the importance of using TCNFs as a reinforcement for the development of PLA-based biocomposites, as ultimately the MOF@Cell filters present superior mechanical properties to those of MOF@PLA filters.

It was demonstrated that even after the acid treatment, the MOF@Cell biocomposite filters present mechanical properties comparable to those of pure and non-treated PLA filters, with both the Young's modulus and toughness values within the same range. The MOF@PLA filters seem to be more affected by the photooxidation reaction induced by the O_3 treatment, as in that case, the drop of the Young's modulus value when
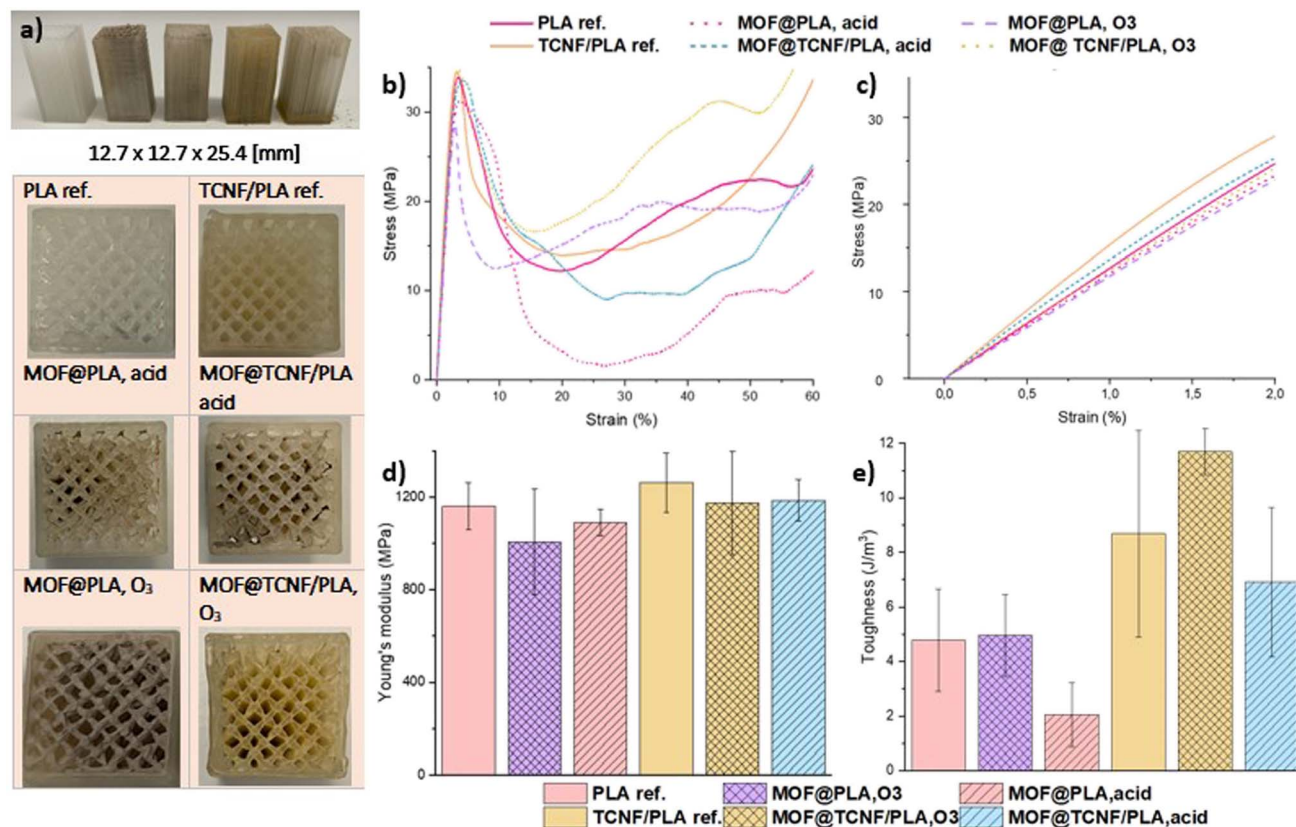

Fig. 4 (a) Overview of the tested samples, (b) stress–strain curves of all of the tested samples, (c) elastic behaviour stage of the stress–strain curves presented in (b), (d) average compressive elastic modulus and (e) average toughness.

compared to that of the inactivated PLA reference filter is approximately 13%. This effect is less pronounced for the O_3 activated TCNF/PLA filters with their Young's modulus value dropping just by 7% when compared to that of the non-treated TCNF/PLA filter. The obtained results indicate that for the MOF@Cell filters the activation mechanism induced on the surface prior to anchoring of the SU-101 adsorbent does not play a significant role, as the mechanical properties in both cases remain the same and are still in the same range as those of the inactivated and pure PLA filters. However, for the PLA filters the activation mechanism seems to be a crucial component affecting their mechanical stability, as the acid activated samples are shown to be nearly twice as resilient to deformation when compared to the O_3 activated samples.

3.3 Functionality of the filters towards removal of metal ions from mine effluent

The adsorption performance of the 3D printed and surface functionalized PLA and TCNF/PLA filters was assessed *via* batch adsorption studies using mine wastewater effluent. The mine effluent was analysed by ICP-MS and it has been shown to contain *i.a.* the following metal ions: V, Cr, Cd, Mn, Co, Ni, Cu, Zn, and As. The 3D printed filters were immersed in the mine effluent and further analysed by the SEM-EDX mapping to assess which of the aforementioned metal ions shows the highest affinity for being adsorbed onto the filter surfaces. During the SEM-EDX mapping, the presence of all of the aforementioned metal ions on the filter surfaces was detected;

however it was evident that some metal ions including *e.g.* Cd, Pb and As are more effectively adsorbed than others (Fig. 5a). The quantitative analysis of the adsorption potential of 3D printed filters by ICP-MS was therefore targeted towards these selected metal ions only, and so, the removal efficiency for Cd^{2+}, Pb^{2+}, As^{3+}, Mn^{2+} and Zn^{2+} was analysed. The obtained results summarizing the removal efficiencies for the selected metal ions after 24 h immersion in mine effluent are presented in Fig. 5b, whereas the removal efficiencies after 1 h immersion are presented in Fig. S4.†

The renewability potential (desorption, acid treatment and re-anchoring) of the filters was demonstrated, as with each adsorption cycle the maximum removal efficiency for various metal ions is not only kept at the same level, but increases. This is direct proof for the stability of the re-functionalized filters and the successful re-anchoring of the MOF, even with omission of the original activation steps. Considering the control sample and Pb^{2+} ion as a first example, it was observed that the removal efficiency for Pb^{2+} was nearly doubled between the first and last adsorption cycle (from 32% in the first adsorption cycle up to 61% in the third adsorption cycle). Before the third adsorption cycle, the control sample underwent two brief acid washes with 10 M HCl in order to remove previously adsorbed metal ions, which seemingly led to improvement of the anchoring of SU-101 onto its surface and resulted in better removal efficiency. The same observation was made for most of the activated filters *e.g.* in the case of the acid-activated TCNF/PLA filter, the removal efficiency for Pb^{2+} increased from 27% in the first adsorption
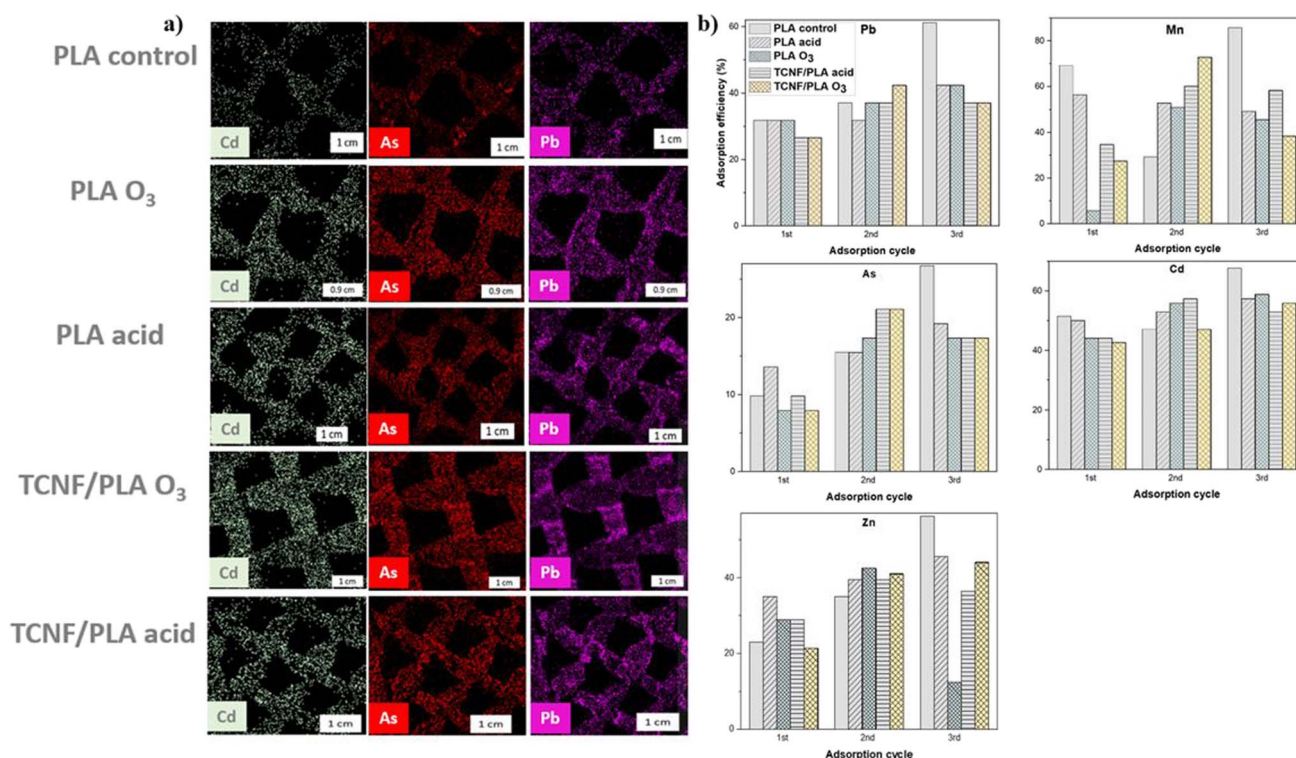

Fig. 5 SEM-EDX images for all of the 3D printed filers with elemental mapping for (a) cadmium (Cd), arsenic (As) and (Pb) and (b) adsorption efficiency for the removal of different metal ions after 24 h immersion measured by ICP-MS.

12390 | *J. Mater. Chem. A*, 2023, **11**, 12384–12394

This journal is © The Royal Society of Chemistry 2023

cycle to 37% in the third adsorption cycle. Additional acid treatment clearly played a key role in enhancing the stability of the filter matrices for consecutive MOF anchoring, by making the surface of the filter more negatively charged,[46] and hence more prone to both interactions with the MOF and adsorption of positively charged metal ions. Interestingly, the primary activation mechanism was not observed to make a significant difference in adsorption performance of the 3D printed filters, as both acid and O_3-activated filters exhibited similar adsorption efficiencies for removal of all tested metal ions. Acid-activated filters have been shown to be slightly more efficient in the removal of ions from contaminated water when compared to O_3-activated ones (*e.g.* for Cd^{2+} removal in the second adsorption cycle, MOF@Cell O_3-activated filters reached removal efficiencies of 53% compared to 57% for MOF@Cell acid-activated filters). All the filters were most efficient in the removal of Mn^{2+} ions with the averaged removal efficiency for three adsorption cycles being 53% and 34% for acid and O_3-activated PLA samples respectively; and 51% and 46% for acid and O_3-activated TCNF/PLA samples, respectively.

Within each separate adsorption cycle all of the filters successfully reduced the concentration of Mn^{2+} ions in water, down to the values well below the maximum Mn^{2+} levels allowed in drinking water according to the European Union standards *i.e.* below 50 µg L^{-1}.[48] The filters have been shown to be least efficient in the removal of As^{3+} ions from water, with average removal efficiencies for this metal ion of around 16 and 14% for acid and O_3-activated MOF@PLA filters, respectively, and 37 and 46% for acid and O_3-activated MOF@Cell filters, respectively. It is noteworthy that the reinforced filters showed twice and trice as high removal efficiencies for As^{3+} when compared to their corresponding MOF@PLA filters. Despite this improvement, even the reinforced filters did not reduce the As^{3+} levels in mine effluent to below the drinking water standards of 10 µg L^{-1}.[48] The removal efficiencies measured for all of the filters within each adsorption cycle are tabulated in Table S2.†

Understanding the underlying mechanisms of heavy metal ion adsorption into MOF structures is important for designing and optimizing MOF-based materials for various applications, including water treatment and environmental remediation. The specific mechanisms of heavy metal ion adsorption into MOF structures can vary depending on the specific properties of the MOF and the metal ion being adsorbed,[49] as well as the environmental conditions such as the pH-value,[50] temperature,[51] and ionic strength.[52] MOFs being porous materials with a large surface area[29] are highly affective for adsorbing metal ions from water through various mechanisms, including physical adsorption through *e.g.* van der Waals interactions[53] and chemisorption.[54] Physical adsorption involves the electrostatic interaction between the metal ions and the surface of the MOF, and is typically enhanced by factors such as the surface area and porosity of the MOF.[55] Chemisorption, on the other hand, involves the formation of chemical bonds between the metal ions and the functional groups on the MOF surface, such as carboxyl, amine, or hydroxyl groups. This mechanism is typically more selective and specific than physical adsorption, as it

requires a certain degree of chemical affinity between the metal ion and the functional group.[55] Moreover, complexation involves the formation of coordination complexes between the metal ions and the metal centres in the MOF structure.[56] This mechanism is typically more selective for certain metal ions and can be influenced by factors such as the metal ion size, charge, and coordination number.[56]

Also, chelation, a form of chemisorption, is a common mechanism of adsorption for MOFs, and it involves the formation of a coordination complex between the metal ion and functional groups on the MOF surface.[57] When metal ions are present in aqueous solutions, they are typically surrounded by a hydration shell consisting of water molecules.[58]

We hypothesize that in the case MOF@Cell and MOF@PLA filters, chelation could be a plausible adsorption mechanism. The phenolate groups on the MOF surface can act as Lewis bases and coordinate with the metal ions, displacing some of the water molecules in the hydration shell. This coordination can result in the formation of stable metal–oxygen bonds, which would lead to the adsorption of metal ions onto the MOF surface. In addition, the phenolate groups can also interact with positively charged metal ions through electrostatic interactions. The negatively charged oxygen atoms in the phenolate groups can attract the positively charged metal ions such as the investigated Cd^{2+}, Mn^{2+}, or Pb^{2+}, forming a bond through coulombic attraction. This process is reversible, as demonstrated by the successful desorption experiments, and depends on factors such as the pH value of the solution and the concentration of metal ions present. Moreover, the integrated porosity of the SU-101 MOF, which contains pores of appropriate size to accommodate metal ions, could be another plausible explanation for successful adsorption of metal ions onto the MOF@3D filters. However, the apparent selectivity suggests a more chemistry-based character of adsorption.

Additionally, the hydrolysis of PLA induced by repeated acid treatment can also lead to the formation of nanopores and roughness on the filter surface, which can further enhance the adsorption capacity of the filter by an enhanced SU-101 anchoring procedure.

3.4 Recovery of the MOF and recyclability of the 3D printed filter – methylene blue removal

MOFs are usually reported as possible adsorbents targeting just one, very specific group of contaminants. The potential of SU-101 for selective separation of metal ions was previously published by Piatek *et al.*[59] whereas Zhang *et al.*[60] reported the potential of SU-101 for being used as a drug carrier. This study aims to combine both of these approaches by using both metal ions and a big molecule contaminant *i.e.* methylene blue (MB), in order to demonstrate the wide potential of SU-101 as an adsorbent as well as the adaptability potential of the developed 3D printed filters. Therefore, after three consecutive adsorption–desorption cycles targeted for the removal of metal ions from mine effluent, the filters were subjected to a final anchoring procedure. At this point, all of the filters were treated three times with 20 vol% NH_4Cl and 10 M HCl solution. SU-101

This journal is © The Royal Society of Chemistry 2023

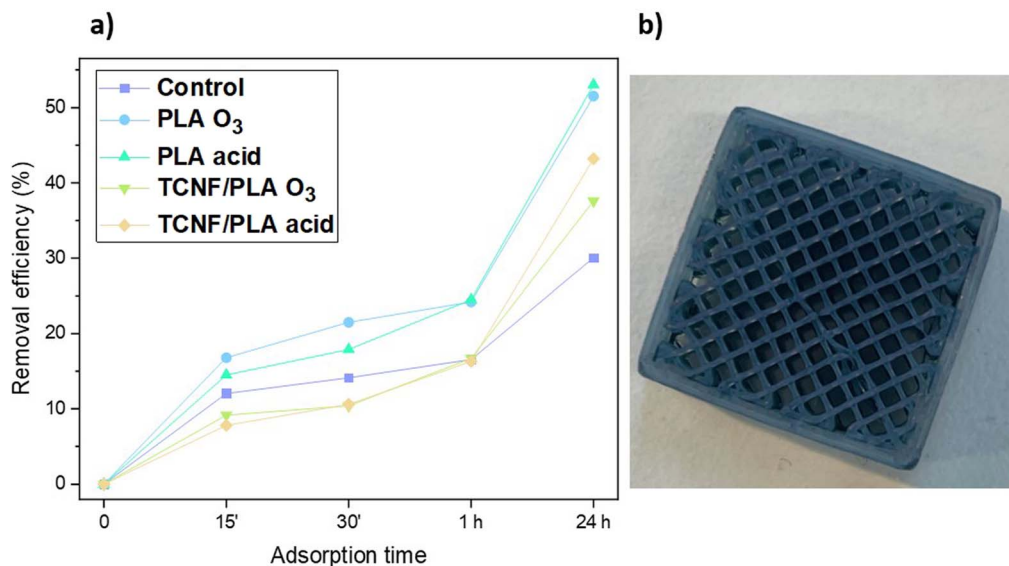*J. Mater. Chem. A*, 2023, **11**, 12384–12394 | **12391**

Fig. 6 (a) Removal efficiencies of MB for all the tested filters and (b) the MOF@Cell filter after MB adsorption.

was re-anchored onto the surface of the filters without an additional activation mechanism. The filters were evaluated for the potential adsorption of cationic dye MB. The adsorption of the dye onto the filter surface is evident, as the filters change colour from brown to deep blue (Fig. 6b) almost immediately after being exposed to the MB solution. The colorimetric method is used to determine the removal efficiency for the filters using the characteristic absorbance peak at 665 nm. The filtrate was collected after 15 min, 30 min, 1 h and 24 h, and the amount of adsorbed dye was calculated based on the remaining dye concentration in the filtrate solution in accordance with the constructed calibration curve (Fig. S1†). The results indicate high potential for using 3D printed filters for MB removal from contaminated water. After 24 h, both of the MOF@PLA filters showed very promising removal efficiencies of 52% and 53% for acid and O_3–activated samples, respectively. The MOF@Cell filters exhibited slightly lower values of 43% and 38% for acid and O_3-activated samples, respectively. These results clearly demonstrate the importance of subjecting the samples to activation prior to anchoring, as indicated by the removal efficiency of the control PLA sample that was a mere 30%. The dye adsorption onto the 3D printed filters occurs primarily due to the interactions between the anchored SU-101 and MB. There are several plausible mechanisms of adsorption that can occur between the MOF and dyes, e.g. electrostatic interaction, hydrogen bonding and π–π stacking between the aromatic rings of the MOF and the MB molecule.[61] The adsorption of MB onto MOF@Cell and MOF@PLA filters occurs most likely via electrostatic interaction between the positively charged dye molecules and the negatively charged adsorbent surface, resulting in the formation of a surface complex on the filters. The adsorption of dyes is dependent on factors such as the pH of the solution,[62] temperature,[63] and the concentration of the dye,[63] and within this study also on the surface properties of the filter, and hence, all these parameters need to be controlled.

In general, for MOF@Cell, the acid-activated samples tend to have higher adsorption efficiency than O_3-activated samples, but additional triple acid treatment conducted during the adsorption–desorption experiments further increases the adsorption efficiency for the removal of metal ions for all the filters and enables successful adsorption of MB. This is due to the fact that PLA is a hydrophilic polymer and consecutive acid treatments lead to hydrolysis of the PLA macromolecule in all of the 3D printed filters resulting in enhanced emergence of hydroxyl and carboxyl groups on the surface.[46] These functional groups provide more anchor points for SU-101 to attach and thus enhance their stability on the surface, as shown by the metal ion adsorption results and increased removal efficiency for each adsorption cycle. The exposed hydroxyl and carboxyl sites can additionally act as binding sites for cationic dyes such as MB.

4. Conclusions

In this study two different types of 3D printed filters were used as a matrix for further functionalization with the bio-based MOF – SU-101. The first type of filter was based on polylactic acid (PLA), which is a biodegradable polymer. The second type of filter was based on a composite of TEMPO-oxidized cellulose nanofibers (TCNFs) and PLA, which was shown to provide enhanced mechanical strength and stability to the 3D printed filters.

Both types of filters were functionalized with the SU-101 MOF using a scalable and sustainable method of either acid hydrolysis using 10 M HCl, or photooxidation using O_3 treatment, resulting in the formation of stable MOF@PLA and MOF@TCNF/PLA (MOF@Cell) filters. Additionally, in order to demonstrate successful functionalization of the 3D printed filters with a biobased SU-101 MOF, the study evaluated the performance of MOF@PLA and MOF@Cell filters for the

12392 | J. Mater. Chem. A, 2023, 11, 12384–12394

This journal is © The Royal Society of Chemistry 2023

removal of heavy metal ions from mine effluent and methylene blue from water. All of the filters, irrespective of the activation mechanism used prior to MOF anchoring, showed high adsorption efficiencies and presented excellent recyclability potential.

Overall, this study shows the potential of utilizing biobased materials and additive manufacturing technology for the development of efficient and sustainable water treatment solutions, and highlights the versatility of the approach in incorporating different types of functional materials, such as MOFs, into the 3D printed filters. The MOF@Cell filters could find applications in various industries, including wastewater treatment, groundwater remediation, and industrial process water purification. Further research should focus on optimizing the fabrication process, exploring the use of different MOF materials and their combinations, and evaluating the long-term performance of the filters under real-world conditions.

Author contributions

NF – conceptualization, methodology, validation, investigation, data curation, writing – original draft, visualization; AM – investigation, data curation, writing original draft; ESG – investigation, data curation, writing original draft, visualization; ZB – data curation, writing – original draft; AKI – conceptualization, data curation; APM – resources, supervision, funding acquisition.

Conflicts of interest

There is no conflict of interest to declare.

Acknowledgements

References

1 M. Kapahi and S. Sachdeva, *Journal of Health and Pollution*, 2019, **9**, 191203.

2 S. Mitra, A. J. Chakraborty, A. M. Tareq, T. B. Emran, F. Nainu, A. Khusro, A. M. Idris, M. U. Khandaker, H. Osman, F. A. Alhumaydhi and J. Simal-Gandara, *J. King Saud Univ., Sci.*, 2022, **34**, 101865.

3 M. Jaishankar, T. Tseten, N. Anbalagan, B. B. Mathew and K. N. Beeregowda, *Interdiscip. Toxicol.*, 2014, **7**, 60–72.

4 H. S. Kim, Y. J. Kim and Y. R. Seo, *J. Cancer Prev.*, 2015, **20**, 232–240.

5 M. Jabłońska-Czapla, K. Nocoń, S. Szopa and A. Łyko, *Environ. Monit. Assess.*, 2016, **188**, 262.

6 R. M. Florea, A. I. Stoica, G. E. Baiulescu and P. Capotă, *Environ. Geol.*, 2005, **48**, 1132–1136.

7 A. S. Ek and I. Renberg, *Journal of Paleolimnology*, 2001, **26**, 89–107.

8 G. Medunić, Ž. Fiket and M. Ivanić, in *Arsenic in Drinking Water and Food*, ed. S. Srivastava, Springer, Singapore, 2020, pp. 183–233.

9 G. Borbély and E. Nagy, *Desalination*, 2009, **240**, 218–226.

10 I. Bakkaloglu, T. J. Butter, L. M. Evison, F. S. Holland and I. C. Hancockt, *Water Sci. Technol.*, 1998, **38**, 269–277.

11 J. Kim, S. Yoon, M. Choi, K. J. Min, K. Y. Park, K. Chon and S. Bae, *J. Cleaner Prod.*, 2022, **330**, 129879.

12 L. Ćurković, Š. Cerjan-Stefanović and T. Filipan, *Water Res.*, 1997, **31**, 1379–1382.

13 D. Georgouvelas, H. N. Abdelhamid, J. Li, U. Edlund and A. P. Mathew, *Carbohydr. Polym.*, 2021, **264**, 118044.

14 A. F. Abdel-Magied, H. N. Abdelhamid, R. M. Ashour, X. Zou and K. Forsberg, *Microporous Mesoporous Mater.*, 2019, **278**, 175–184.

15 R. M. Ashour, H. N. Abdelhamid, A. F. Abdel-Magied, A. A. Abdel-Khalek, M. M. Ali, A. Uheida, M. Muhammed, X. Zou and J. Dutta, *Solvent Extr. Ion Exch.*, 2017, **35**, 91–103.

16 D. Georgouvelas, H. N. Abdelhamid, J. Li, U. Edlund and A. P. Mathew, *Carbohydr. Polym.*, 2021, **264**, 118044.

17 T. G. Danis, T. A. Albanis, D. E. Petrakis and P. J. Pomonis, *Water Res.*, 1998, **32**, 295–302.

18 K. Imamura, E. Ikeda, T. Nagayasu, T. Sakiyama and K. Nakanishi, *J. Colloid Interface Sci.*, 2002, **245**, 50–57.

19 H. Ahmad, A. R. A. Abdulwahab, B. H. Koo and R. A. Khan, *ACS Omega*, 2022, **7**, 3044–3051.

20 R. Wang, W. Zhang, L. Zhang, T. Hua, G. Tang, X. Peng, M. Hao and Q. Zuo, *Environ. Sci. Pollut. Res.*, 2019, **26**, 1595–1605.

21 M. Deravanesiyan, M. Beheshti and A. Malekpour, *J. Ind. Eng. Chem.*, 2015, **21**, 580–586.

22 A. Mahapatra, B. G. Mishra and G. Hota, *J. Hazard. Mater.*, 2013, **258–259**, 116–123.

23 E. Guibal, R. Lorenzelli, T. Vincent and P. L. Cloirec, *Environ. Technol.*, 1995, **16**, 101–114.

24 A. M. Burke, J. P. Hanrahan, D. A. Healy, J. R. Sodeau, J. D. Holmes and M. A. Morris, *J. Hazard. Mater.*, 2009, **164**, 229–234.

25 H. Hu, Z. Wang and L. Pan, *J. Alloys Compd.*, 2010, **492**, 656–661.

26 V. K. Gupta and Suhas, *J. Environ. Manage.*, 2009, **90**, 2313–2342.

27 K. Kadirvelu and C. Namasivayam, *Adv. Environ. Res.*, 2003, **7**, 471–478.

28 K. Kadirvelu, K. Thamaraiselvi and C. Namasivayam, *Sep. Purif. Technol.*, 2001, **24**, 497–505.

29 H. Furukawa, K. E. Cordova, M. O'Keeffe and O. M. Yaghi, *Science*, 2013, **341**, 1230444.

30 Y. Peng, H. Huang, Y. Zhang, C. Kang, S. Chen, L. Song, D. Liu and C. Zhong, *Nat. Commun.*, 2018, **9**, 187.

This journal is © The Royal Society of Chemistry 2023

J. Mater. Chem. A, 2023, **11**, 12384–12394 | **12393**

31 F. Ahmadijokani, S. Tajahmadi, A. Bahi, H. Molavi, M. Rezakazemi, F. Ko, T. M. Aminabhavi and M. Arjmand, *Chemosphere*, 2021, **264**, 128466.

32 J. Li, X. Wang, G. Zhao, C. Chen, Z. Chai, A. Alsaedi, T. Hayat and X. Wang, *Chem. Soc. Rev.*, 2018, **47**, 2322–2356.

33 E. S. Grape, J. G. Flores, T. Hidalgo, E. Martínez-Ahumada, A. Gutiérrez-Alejandre, A. Hautier, D. R. Williams, M. O'Keeffe, L. Öhrström, T. Willhammar, P. Horcajada, I. A. Ibarra and A. K. Inge, *J. Am. Chem. Soc.*, 2020, **142**, 16795–16804.

34 I. Gibson, D. Rosen, B. Stucker and M. Khorasani, *Additive Manufacturing Technologies*, Springer International Publishing, Cham, 2021.

35 V. Mazzanti, L. Malagutti and F. Mollica, *Polymers*, 2019, **11**, 1094.

36 N. Fijoł, A. Aguilar-Sánchez, M.-X. Ruiz-Caldas, J. Redlinger-Pohn, A. Mautner and A. P. Mathew, *Chem. Eng. J.*, 2023, **457**, 141153.

37 Z. Liu, Y. Wang, B. Wu, C. Cui, Y. Guo and C. Yan, *Int. J. Adv. Manuf. Technol.*, 2019, **102**, 2877–2889.

38 L.-T. Lim, R. Auras and M. Rubino, *Prog. Polym. Sci.*, 2008, **33**, 820–852.

39 G. Spinelli, P. Lamberti, V. Tucci, R. Ivanova, S. Tabakova, E. Ivanov, R. Kotsilkova, S. Cimmino, R. Di Maio and C. Silvestre, *Composites, Part B*, 2019, **167**, 467–476.

40 W. Wang, B. Zhang, M. Li, J. Li, C. Zhang, Y. Han, L. Wang, K. Wang, C. Zhou, L. Liu, Y. Fan and X. Zhang, *Composites, Part B*, 2021, **224**, 109192.

41 Z. Wang, J. Xu, Y. Lu, L. Hu, Y. Fan, J. Ma and X. Zhou, *Ind. Crops Prod.*, 2017, **109**, 889–896.

42 K. M. N'Gatta, H. Belaid, J. El Hayek, E. F. Assanvo, M. Kajdan, N. Masquelez, D. Boa, V. Cavaillès, M. Bechelany and C. Salameh, *Sci. Rep.*, 2022, **12**, 21244.

43 Q. Wang, C. Ji, L. Sun, J. Sun and J. Liu, *Molecules*, 2020, **25**, 2319.

44 A. Aguilar-Sanchez, B. Jalvo, A. Mautner, S. Nameer, T. Pöhler, T. Tammelin and A. P. Mathew, *J. Membr. Sci.*, 2021, **620**, 118842.

45 N. Fijoł, H. N. Abdelhamid, B. Pillai, S. A. Hall, N. Thomas and A. P. Mathew, *RSC Adv.*, 2021, **11**, 32408–32418.

46 K. Kim, M. C. Ratri, G. Choe, M. Nam, D. Cho and K. Shin, *PLoS One*, 2020, **15**, e0231475.

47 J. Choi, P. J. H. Kim, J. Seo, J. Kwon, S. Lee and T. Song, *Adv. Eng. Mater.*, 2018, **20**, 1700901.

48 European Union, Directive (EU) 2020/2184 of the European Parliament and of the Council of 16 December 2020 on the Quality of Water Intended for Human Consumption, *Off. J. Eur. Union*, 2020, **435**, 1–62.

49 S.-W. Lv, J.-M. Liu, C.-Y. Li, N. Zhao, Z.-H. Wang and S. Wang, *Chem. Eng. J.*, 2019, **375**, 122111.

50 Z. Seyfi Hasankola, R. Rahimi, H. Shayegan, E. Moradi and V. Safarifard, *Inorg. Chim. Acta*, 2020, **501**, 119264.

51 B. Panella, M. Hirscher, H. Pütter and U. Müller, *Adv. Funct. Mater.*, 2006, **16**, 520–524.

52 S. Ul Mehdi and K. Aravamudan, *Mater. Today: Proc.*, 2022, **61**, 487–497.

53 I. Ahmed and S. H. Jhung, *J. Hazard. Mater.*, 2016, **301**, 259–276.

54 T. A. Vu, G. H. Le, C. D. Dao, L. Q. Dang, K. T. Nguyen, Q. K. Nguyen, P. T. Dang, H. T. K. Tran, Q. T. Duong, T. V. Nguyen and G. D. Lee, *RSC Adv.*, 2014, **5**, 5261–5268.

55 L. Rani, J. Kaushal, A. L. Srivastav and P. Mahajan, *Environ. Sci. Pollut. Res.*, 2020, **27**, 44771–44796.

56 N. A. Khan and S. H. Jhung, *J. Hazard. Mater.*, 2017, **325**, 198–213.

57 Z. Sun, C. Tian, T. Yang, J. Fu, H. Xu, Y. Wang and Z. Lin, *Sep. Purif. Technol.*, 2022, **301**, 121946.

58 S. Obst and H. Bradaczek, *J. Phys. Chem.*, 1996, **100**, 15677–15687.

59 J. Piątek, T. M. Budnyak, S. Monti, G. Barcaro, R. Gueret, E. S. Grape, A. Jaworski, A. K. Inge, B. V. M. Rodrigues and A. Slabon, *ACS Sustainable Chem. Eng.*, 2021, **9**, 9770–9778.

60 Q. Zhang, Y. Liu, Z. Wang, P. Wang, Z. Zheng, H. Cheng, X. Qin, X. Zhang, Y. Dai and B. Huang, *J. Colloid Interface Sci.*, 2022, **617**, 578–584.

61 A. A. Alqadami, Mu. Naushad, Z. A. Alothman and T. Ahamad, *J. Environ. Manage.*, 2018, **223**, 29–36.

62 Kirandeep, Sushila, A. Sharma, S. C. Sahoo, G. Kumar, S. K. Mehta and R. Kataria, *J. Mol. Struct.*, 2021, **1226**, 129327.

63 E. Haque, J. W. Jun and S. H. Jhung, *J. Hazard. Mater.*, 2011, **185**, 507–511.

12394 | *J. Mater. Chem. A*, 2023, **11**, 12384–12394

This journal is © The Royal Society of Chemistry 2023